Eur. Phys. J. B **30**, 117–123 (2002)
DOI: 10.1140/epjb/e2002-00365-8

THE EUROPEAN PHYSICAL JOURNAL B

Ab initio calculation of Electron Energy Loss spectra of clean and 1ML Fe-covered Ni(111)

R. Capelli[1,a], P. Monachesi[2,b], R. Del Sole[1], and G.C. Gazzadi[2]

[1] Dipartimento di Fisica - Università di Roma, "Tor Vergata" and Istituto Nazionale per la Fisica della Materia, 00133 Roma, Italy
[2] Dipartimento di Fisica - Università dell'Aquila and Instituto Nazionale di Fisica della Materia, 67010 l'Aquila, Italy
[3] Istituto Nazionale per la Fisica della Materia and Dipartimento di Fisica, Università di Modena e Reggio Emilia, via G. Campi 213, 41100 Modena, Italy

Received 10 July 2002
Published online 19 November 2002 –

Abstract. The dielectric and the loss functions of Ni(111) are calculated by the Full Potential Linear Muffin Tin Orbitals (FPLMTO) *ab initio* method whithin the three-layers model (vacuum/surface/bulk). Particular attention is devoted to determine surface and bulk state contributions to the spectra. Good agreement is found with recent experimental EELS data on the Fe-covered Ni(111) surface.

PACS. 71.28.+d Narrow-band systems; intermediate-valence solids – 71.20.-b Electron density of states and band structure of crystalline solids – 78.20.-e Optical properties of bulk materials and thin films

1 Introduction

Electron Energy Loss Spectroscopy (EELS) is a technique widely used to study surfaces and overlayers of many materials [1]. Compared to optical spectroscopy, *e.g.* Reflectance Anisotropy Spectroscopy (RAS) [2], it has the advantage of a greater sensitivity to the surface which compensates for its worse energy resolution and greater invasivity. A recent development of this technique, the anisotropic [3] surface EELS, yields surface loss anisotropies two orders of magnitude larger than those obtained by RAS.

Theoretical progress in the interpretation of EELS spectra is, however, scarce. On one side, modeling an EELS spectrum usually assumes restrictions to the transferred momentum not always fulfilled in the experiments [1,4]. On the other side, there is the need of an accurate *ab initio* calculation of the spectral functions. It is, therefore, desirable to improve both these aspects. The EEL spectrum in the bulk is proportional to the loss function $f(\boldsymbol{q},\omega)$, defined in terms of the dielectric function $\epsilon(\boldsymbol{q},\omega)$ as:

$$f = -\mathrm{Im}(\epsilon^{-1}) = \frac{\epsilon_2}{\epsilon_1^2+\epsilon_2^2} \qquad (1)$$

where the subscripts $1,2$ indicate the real and imaginary part of $\epsilon(\boldsymbol{q},\omega)$, respectively. $\boldsymbol{q}$ and ω, understood in (1), are the wave vector and energy transferred to crystal electrons [1], respectively. If $\boldsymbol{q}$ is small with respect to the characteristic wavectors of the system, *e.g.* the reciprocal lattice vectors, the dependence of ϵ on it can be neglected and the loss function in (1) is obtained in terms of the optical dielectric function, $\epsilon(0,\omega)$. Usually, calculations are carried out within this scheme, the so-called dipole approximation, and neglecting local-field effects [3,4].

The structure of equation (1) makes the result very sensitive to vanishing or small denominators. Therefore a great accuracy in ϵ_1 and ϵ_2 must be achieved in the calculations. Recently several calculations have been carried out for the EELS spectra of bulk Pd [5–7]. The attempt to improve the agreement with existing experiments [8] has been successful, even neglecting local field effects , by increasing substantially the accuracy of the adopted *ab initio* calculations to attain a better convergence of ϵ in a wide energy range. Among others, the Full Potential Linear Muffin Tin Orbitals (FP-LMTO) method [9,10] turned out to be a very efficient *ab initio* scheme for the calculations of optical functions of both bulk metals [5] and metal surfaces [11].

In the present work, we apply the FP-LMTO method to interpret the results obtained by surface EELS measurements [12] in systems of Fe overlayers on the Ni (111) surface. We adopt essentially the *three-layer* model [13] (bulk-surface-vacuum) to represent the interface and use

[a] *Present address*: Istituto per lo Studio dei materiali Nanostrutturati, Unità di Bologna CNR, Via Gobetti 101, Bologna, Italy
[b] e-mail: patrizia.monachesi@roma2.infn.it

the corresponding version of equation (1). We also have to reconsider the usual dipole approximation, where the momentum transfer is assumed to be negligible. In fact, large momenta are transferred to crystal electrons in the EELS measurements [12] to be described by our calculations.

The general theoretical framework, along with computational details of the FP-LMTO method and a short review of the theory of surface EELS are given in Section 2. We show how the dipole approximation can be used to cope with the present situation of a large momentum transfer. The comparison with experimental data is discussed in Section 3 and the conclusions are drawn in Section 4.

2 Method of calculation

2.1 Electronic structure

The calculation of the electronic structure and of the optical functions in bulk Ni and at interfaces is done within the Full Potential Linear Muffin Tin Orbital [9,10] method in the framework of Density Functional Theory (DFT) [14], using the exchange-correlation potential of von Barth-Hedin [15] in the Local Density approximation (LDA). Many-body effects beyond DFT-LDA (self-energy, electron-hole interaction effects) have been shown to be small in noble metals [16]. We assume them to be small also in Ni. This is an itinerant ferromagnet below $T_C = 613$ K. The exchange splitting amounts to 100–300 meV and affects very little the minority- and majority-spin electronic structure at the (111) surface [17,18]. This splitting is surely overwhelmed by the intrinsic broadening of the EELS spectra. We therefore perform calculations for the paramagnetic phase within the DFT-LDA scheme.

As usual, the repeated slab scheme is assumed to model the bulk-surface-vacuum system, representing the truncated solid. The slab is made up by a fixed yet arbitrary number of atomic layers, symmetrically added on the two sides of a central layer and terminated by a fixed yet arbitrary number of vacuum layers. The optimal dimension of the slab is that for which the quantity of interest (*e.g.* total energy, density of state, dielectric function etc.) converges. In this scheme, the slab replaces the bulk unit cell. In the FP-LMTO method the unit cell is divided into finite spherical regions (the Muffin Tin Spheres), centered around each atom, embedded in the so-called interstitial region. The Kohn-Sham equations of DFT have different solutions within the spheres and in the interstitial region. These solutions are then matched at each sphere boundary in a continuous and differentiable way, forming the muffin tin orbitals centered on the muffin tin spheres. The muffin tin orbitals are the sought-for basis functions, atomic-like inside the MT spheres and given by linear combinations of Hankel or Neuman functions outside. The latter ones, also called *tails* or envelope functions are denoted by the κ^2-value (negative or positive) of the kinetic energy. The FP-LMTO method is very appropriate for metallic systems since its basis set, basically a localized one, describes well narrow states like the d's. As pointed out in detail elsewhere [5], the number of basis functions included in the expansion of the crystal wave function determines the accuracy of the calculation. In the case of optical functions the larger the basis the more extended the energy range where optical transitions are included. The minimum basis set includes, for each atomic species, all the occupied orbitals in the neutral atomic configuration and one single *tail* for each atomic orbital.

The atomic configuration of Ni is [Ar]$3d^8 4s^2$. In our calculations the basis set is made by the Ar core, able to relax but not to hybridize, the valence configuration $3d^8 4s^2$ and the six 4p orbitals to account for empty states. Two different tails are considered for each state. An analogous basis set turned out to be enough to reproduce correctly the dielectric function of Cu and Ag (110) surface up to 7 eV [11]. A slab made by 11 layers of Ni(111) plus 6 vacuum layers satisfies the requirements of convergence for the dielectric function of the interface [11].

The positions of all atoms in the slab are a primary input of the calculations. Most highly symmetric clean surfaces of noble metals do not reconstruct. Hence we assume ideal positions for the surface Ni atoms. When atoms are adsorbed on the surface, there may be relaxation and/or reconstruction: the atomic positions are to be determined carefully, experimentally or by molecular-dynamics techniques [19]. The determination of the atomic structure of the first Fe layers growing on Ni(111) has been controversial. Theoretical calculations [27] at 0 K indicated that the energetically favored adsorption site was the hcp-hollow and not the fcc one. A sub-sequent experimental investigation [28] was performed with energy-scanned Photoelectron Diffraction (PD) on a 0.6 ML film, grown at 130 K. The results contradicted the previous findings, showing that the Fe atoms were adsorbed at the fcc-hollow sites, with Fe-Ni interlayer distance slightly expanded with respect to the Ni-Ni one. In the present work, we use as the input structure for the Fe layer the one obtained by a recent experimental work [29] on Fe/Ni(111) films, studied by angle-scanned PD in the 1-18 ML coverage range. For the case of 1 Fe monolayer, which is considered here, Fe atoms are assigned the atomic positions of the first missing Ni layer, *i.e.* at the fcc-hollow sites.

The calculations of the electronic band structure for the bulk and the (111) surface of Ni have been done considering 47 and 36 k-points in the 3-D and 2-D irreducible Brillouin Zone, respectively, to determine the charge densities. The lattice parameter has been taken [23] $a = 6.65$ a.u. In Figure 1 we show the energy bands of the clean (111) Ni surface along two high-symmetry directions of the 2-D Brillouin Zone. The flatness and position of the d bands below the Fermi level ($E_F = 0$ in the figure) will be exploited for the evaluation of the EEL spectra in the next section.

2.2 EEL spectra

Within the dipole and the Random Phase Approximations (RPA), the imaginary part of the diagonal component ii

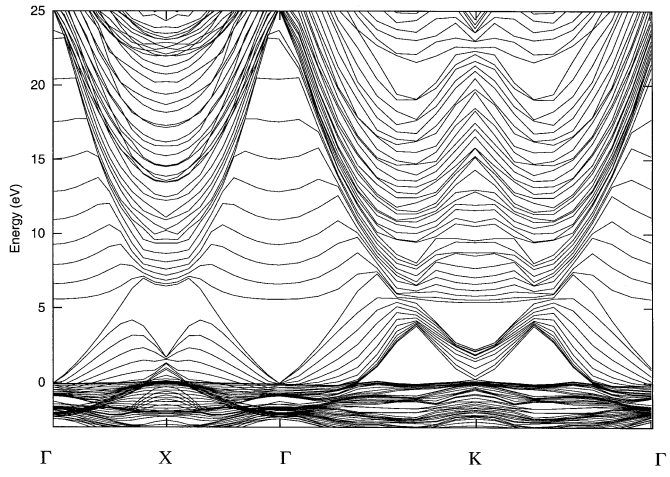

Fig. 1. Surface band structure of Ni(111). **K** is the corner of the 2D hexagonal BZ and **X** is the middle point of the edge.

of the dielectric tensor is calculated as [20]:

$$\epsilon_{ii}(\omega) = 1 - \frac{4\pi e^2}{m^2\hbar\omega}\sum_k\sum_{l_{occ}}\sum_{n_{unocc}}\frac{1}{\omega_{nl}}\left(\frac{|\Pi^i_{ln}|^2}{\omega-\omega_{nl}+\mathrm{i}\delta} + \frac{|\Pi^i_{ln}|^2}{\omega+\omega_{nl}+\mathrm{i}\delta}\right) \quad (2)$$

where $|\Pi_{ln}|$ is the momentum–operator matrix element between the l occupied (valence) and n unoccupied (conduction) electronic states.

The real part, ϵ_1 is then obtained by Kramers-Kronig transforming ϵ_2 [20]. In this framework we evaluated $\epsilon(\omega)$ of the (111) surface, clean and Fe covered, and of bulk Ni from the *ab initio* calculated interband dipolar transitions among valence and conduction electronic states according to equation (2). Compared to the evaluation of the electronic structure, the calculation of $\epsilon(\omega)$, involving the crystal wave functions, requires an increased number of k-points in the interpolation scheme of the tetrahedron method [21]. We used 752 and 256 k-values in the irreducible 3-D and 2-D Brillouin Zone, respectively. The intraband part of ϵ in the bulk has been evaluated, as usual, from the Drude formulas with experimental values of the plasma frequency and relaxation time [22] amounting to 9 eV and 20 eV^{-1}, respectively [23]. The same values have been used, as an approximation, also for the surface considered here. This procedure may induce only negligible errors in the frequency range of interest here, that is above 4 eV. From the dielectric function, the Electron Energy Loss in the three-layers model can be calculated using a formula, analogous to equation (1), which is given below [4].

Before going into the details of the three-layer model of the Loss function, however, we have to discuss the argument that allows us to apply the dipole approximation for the optical transitions also in the present case. In the EELS experiment of reference [12] the incident electron beam was normal to the (111) surface of a Ni sample. The scattered electrons were detected by a cylindrical mirror analyser at an average angle of 20 degrees with respect to the surface normal with an angular acceptance of 10 degrees. The energy of the incident electrons was 150 eV. In these experimental conditions the values of the wave vectors $\boldsymbol{q}$ transferred by the incident electron to the surface are larger than the first Brillouin Zone boundaries and spread over one or more Brillouin Zones. Therefore, it seems no longer possible to interpret the experimental data with the imaginary part of the surface dielectric function $\epsilon_2(\boldsymbol{q},\omega)$ calculated in the limit $\boldsymbol{q}\to 0$. Nevertheless, as shown below, taking into account the details of the band structure enables us to keep the $\boldsymbol{q}\to 0$ limit valid in practice. In fact, inspection of Figure 1 suggests the following considerations. Let us consider a non vertical transition between a given occupied (at $\boldsymbol{k}_i$) and unoccupied (at $\boldsymbol{k}_f$) band. The transition energy is almost the same as that of the vertical transition across the same bands at $\boldsymbol{k}_f$. The experimental spectrum embodies, at a given loss energy, many such non-vertical transitions, each of them corresponding to a transferred q-value within the acceptance of the analyser. Due to the flatness of the occupied d bands, all these transitions occur essentially at the same energy, although with different probabilities (*i.e.* matrix elements). Therefore, our approximation consists in taking a transition probability at zero momentum instead of the correctly averaged one. We expect this to be qualitatively correct but with quantitative energy discrepancies of the order of the dispersion of the d bands (about 1 eV) between experimental and theoretical spectra. The results shown in the next sections confirm the soundness of this approach.

The calculation of the loss function and the EEL spectra [4] within the three-layers model starts from considering the probability $P(\boldsymbol{k},\boldsymbol{k'})$ that an incoming electron with momentum $\boldsymbol{k}$ is scattered to a state of momentum $\boldsymbol{k'}$, loosing an energy $\hbar\omega$, which is given by:

$$P(\boldsymbol{k},\boldsymbol{k'}) = \frac{2}{(ea_0\pi)^2}\frac{1}{\cos\phi_i}\frac{K'}{K}\frac{q_y}{|q_y^2+q_z^2|}Img(q_y,\omega), \quad (3)$$

where

$$Img(q_y,\omega) = \mathrm{Im}\frac{2}{1+\epsilon_{\mathit{eff}}(q_y,\omega)} = f(q_y,\omega). \quad (4)$$

This equation is the surface *three-layer* model version of equation (1). It contains the effective dielectric function of the three–layer system:

$$\epsilon_{\mathit{eff}}(q_y,\omega) = \epsilon_s\frac{\epsilon_b\cos(q_zd_s) - \mathrm{i}\epsilon_s\sin(q_zd_s)}{\epsilon_s\cos(q_zd_s) - \mathrm{i}\epsilon_b\sin(q_zd_s)}, \quad (5)$$

which is a sort of average of the dielectric function over surface and bulk, depending on q_z, the component perpendicular to the surface of the transferred momentum. q_z is proportional to q_y, the surface component of the transferred momentum, according to

$$q_z \equiv q_y(-\epsilon_y/\epsilon_z)^{1/2} = iq_y(\epsilon_y/\epsilon_z)^{1/2}. \quad (6)$$

Finally, the surface dielectric function ϵ_s is given by:

$$\epsilon_s = \sqrt{\epsilon_y \epsilon_z}, \tag{7}$$

i.e., the geometrical average of the two components of the dielectric tensor, ϵ_y and ϵ_z in the scattering plane. This formula has been first derived by Ibach and Mills for an isotropic surface [1] (for which $\epsilon_y = \epsilon_z$) and then generalized to an anisotropic surface by Selloni and Del Sole [4].

In our case, q_y and hence q_z are very large. Moreover, q_z has a predominant imaginary part so that the terms $\sin(q_z d_s)$ and $\cos(q_z d_s)$ behave like hyperbolic functions. Hence, the large q_z limit is easily obtained by neglecting the vanishing exponentials therein, getting:

$$\lim_{q_y \to \infty} \epsilon_{eff}(q_y, \omega) = \epsilon_s. \tag{8}$$

This result is very reasonable: for large momentum transfer q_z perpendicular to the surface, the electron-surface interaction is strongly local, so that only the surface layer determines the loss probability, while the substrate is not effective. The surface dielectric function defined in equation (7) accounts for the anisotropy of the surface, where the z direction (the surface normal) is different from the directions on the surface (x and y). Here the plane of scattering is assumed to be the yz plane, which leads to the presence of ϵ_y in (6). A last remark is about the kinematical factor (the fractions on the right hand side of (3)): in the experimental conditions of reference [12], the kinematical factor is almost constant, and therefore has not been included in the calculations discussed below.

It is possible to separate electronic transitions into surface-to-surface (ss), surface-to-bulk (sb), bulk-to-surface (bs) and bulk-to-bulk (bb) state transitions in the calculation of ϵ_2 [11,24], to interpret the structures in ϵ and f in terms of transitions involving bulk and/or surface states. On the other hand, starting from ϵ_2 of the Ni slab and of bulk Ni, we obtain the surface dielectric function, ϵ_{surf}, within the three-layers model using the linear relation:

$$N_{surf}\epsilon_{surf} = N_{slab}\epsilon_{slab} - (N_{slab} - N_{surf})\epsilon_{bulk}. \tag{9}$$

The parameters N_{slab} and N_{surf} indicate respectively the total number of layers of the slab and the number of layers assigned to the surface. Having calculated the surface dielectric function from (9), and its ss, sb, and bs components (which coincide with the slab ones, since surface states do not affect ϵ_b), we can find the bulk-bulk transition contribution, $\epsilon_{surf}^{bulk \to bulk}$, to the surface dielectric function:

$$\epsilon_{surf} = \epsilon_{slab}^{surf \to surf} + \epsilon_{slab}^{surf \to bulk} + \epsilon_{slab}^{bulk \to surf} + \epsilon_{surf}^{bulk \to bulk}. \tag{10}$$

The meaning of the, seemingly odd, definition $\epsilon_{surf}^{bulk \to bulk}$ is the following one: bulk states of course are present not only in bulk, but also near the surfaces, although modified by the surface potential; transitions across them can of course occur also in the surface region [24]. In a slab calculation this situation leads to a bb contribution to the slab dielectric function and to surface optical properties, often called the 'surface-modified bulk-state contribution to surface optical properties' [24]. In our notation, $\epsilon_{surf}^{bulk \to bulk}$ is the bulk-state contribution to the surface dielectric function. It can be extracted from (10), since the lhs can be calculated from (9), and the first three terms on the rhs are obtained from the slab calculation.

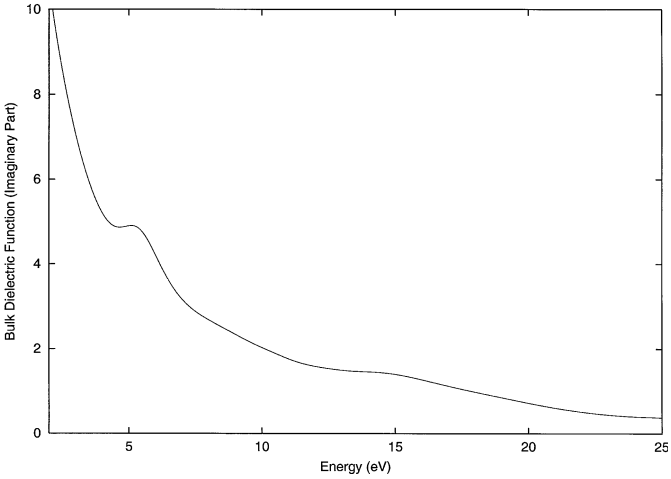

Fig. 2. Calculated imaginary part of the dielectric function of bulk Ni.

All the previous relations are valid for the imaginary and real parts of the y and z components of the dielectric tensor: the former is worked out directly, whereas the latter is obtained by Kramer-Kronig transforms.

The knowledge of the surface dielectric function fully disentangled in its surface and bulk terms is very helpful to get information about the origin of the structures in the EELS spectra.

3 Results and discussion

The starting point for the calculation of the EELS spectra using equations (4) and (5) is the bulk and slab dielectric function, whose imaginary parts are plotted in Figures 2 and 3, respectively. For the slab are shown the two different spectra corresponding to $\boldsymbol{q}$-directions parallel and perpendicular to the surface.

We used equation (9), fixing the number of the surface layers equal to 4 [25], to obtain the imaginary part of the surface dielectric function from the spectra shown in Figures 2 and 3, for the y direction, parallel to the surface, and for the z direction, perpendicular to it. The resulting imaginary part of the surface dielectric function ϵ_s, the geometrical average of equation (7), is shown in Figure 4, while its real part is shown in Figure 5. The main structures show up at 6 eV and 15 eV for the imaginary part and at 5 eV and 14 eV for the real part. Moreover, from Figure 5 we see that at 10 eV the real part of the

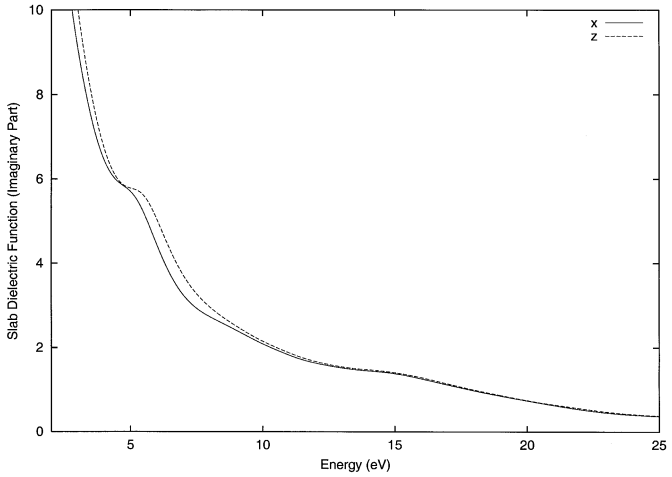

Fig. 3. Calculated imaginary part of the dielectric function of the Ni(111) slab.

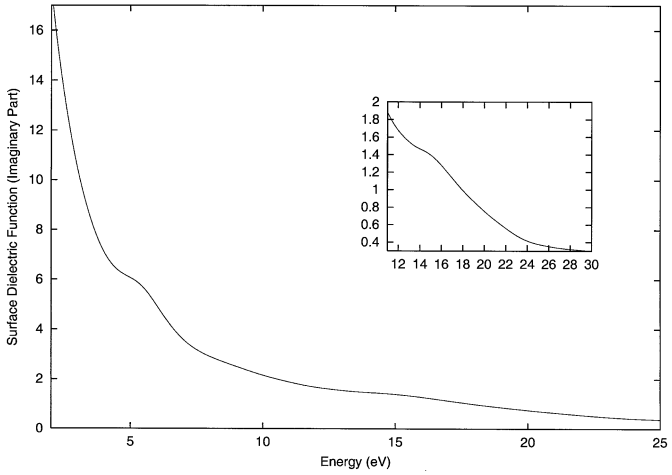

Fig. 4. Calculated imaginary part of the surface dielectric function of Ni(111) (see Eq. (7)).

surface effective dielectric function becomes equal to -1, so that, according to equation (4), we expect to find the surface-plasmon peak in the spectrum near this energy. To calculate EELS spectra we used equation (4). The second derivative, changed of sign, of the EEL spectrum with respect to the energy, is the function $-f''$, shown in Figure 6, that corresponds to the experimental data of reference [12]. We can see that, within the expected error of $\simeq$ 1 eV, due to the d-band dispersion, there is good agreement between f'' calculated (see Fig. 6) and measured (see Fig. 7).

We try now to understand the origin of the structures in Figure 6. According to the physical interpretation of the maxima and minima of the $-f''$ function discussed in reference [26] we assign, to a first approximation, each minimum to an absorption peak and each maximum to an EELS peak. The latter point is also apparent from the two curves related to the clean surface in Figure 6. We can recognize in $-f$", shown in Figure 6, maxima at 4.5 eV, 7.5 eV, 10.5 eV, 11.5 eV, 17.5 eV and 21.5 eV.

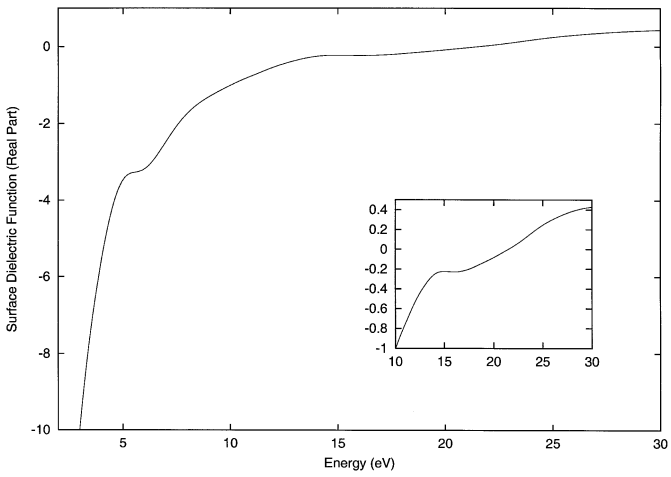

Fig. 5. Calculated real part of the surface dielectric function of Ni(111) (see Eq. (7)).

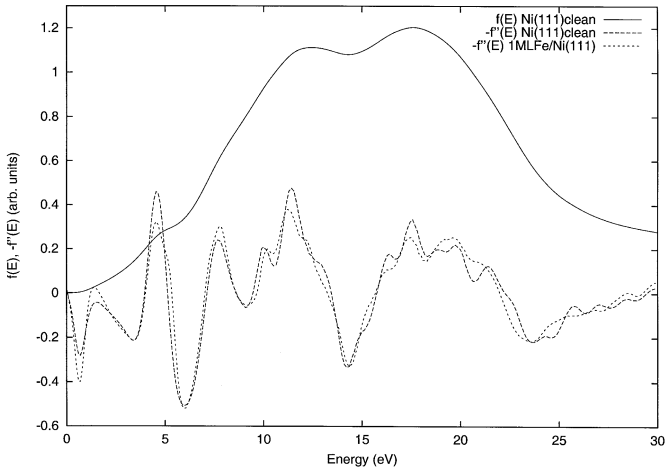

Fig. 6. Calculated second derivative of the loss function of Ni(111) (short dashed) and Fe/Ni(111) (long dashed). Loss function of Ni(111) (solid).

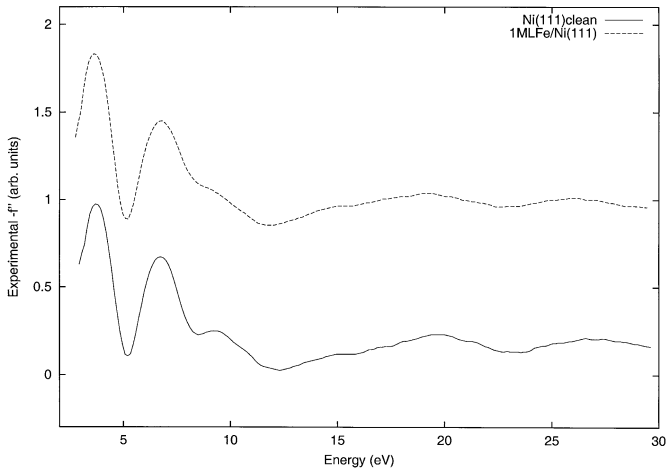

Fig. 7. Experimental second derivative of the loss function for the clean and 1ML Fe-covered Ni(111) surface from reference [12].

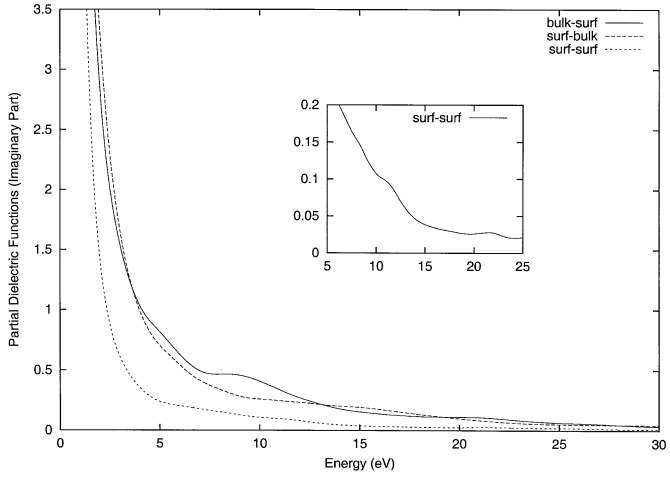

Fig. 8. Imaginary part of the dielectric function calculated for the bulk-surface, surface-bulk, surface-surface transitions of the Ni(111) slab.

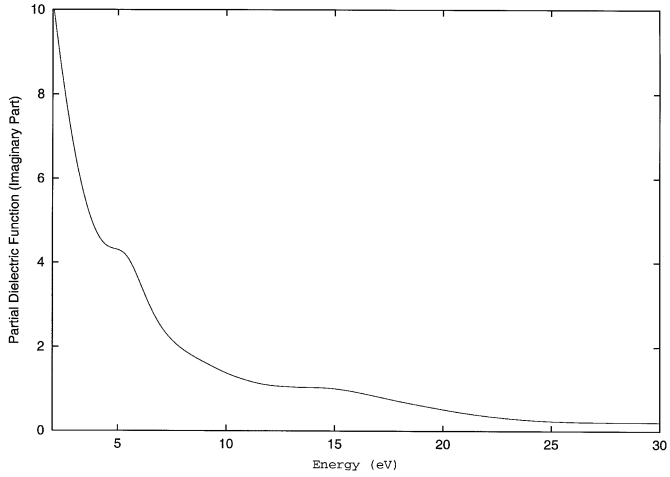

Fig. 9. Contribution to the surface imaginary part of the dielectric function of bulk-bulk transitions.

The decomposition of the surface dielectric function into the contributions of s-s, s-b, b-s and b-b transitions is shown in Figures 8 and 9. We can now interpret the structures appearing in the loss function second derivative of Figure 6. The maxima at 4.5 eV and $\simeq$ 8 eV, corresponding to the first two large peaks in Figure 7, are due to b-b transitions (see Fig. 9). The structures between 10 and 11 eV, probably washed out by a larger broadening in the experiment, are due to s-s transitions (see Fig. 8). The peak above 11 eV, corresponding to the large shoulder at $\simeq$ 10 eV in the experimental curve of Figure 7, is due to the surface plasmon ($\epsilon_s = -1$, see Fig. 5). The broad structure between 14 and 24 eV comes from a region where $Re(\epsilon_s)$ is close to zero (see Fig. 5) and the imaginary part of the dielectric function has also some structures (see Fig. 4). We could interpret this broad peak as the "bulk plasmon", calculated, however, with the surface dielectric function. Notice that the surface and "bulk" plasmons produce the most important features in the loss function, always shown in Figure 6. Our findings generally agree with the experimental ones of Figure 7. The discrepancies in the energy positions are probably due to the neglect of effects beyond DFT-LDA [11]. We stress that our "bulk" structures are actually due to b-b transition effects on the surface dielectric function defined in (7).

Finally, the calculated second derivative of the loss function for the Fe-covered surface is compared to that of the clean surface in Figure 6. The experimental trends of Figure 7 are confirmed: the first peak broadens, while the shoulder at $\simeq$ 10 eV, due to the surface plasmon of Ni, weakens. The latter finding can be understood in terms of a shadowing effect of the Fe overlayer on the Ni substrate, since the present experimental arrangement is extremely sensitive to the surface. A similar effect occurs for the broad structure around 20 eV, due to the 'bulk' plasmon of Ni.

4 Conclusion

We have carried out an *ab initio* calculation of loss spectra for the Ni(111) surface, both clean and covered by one monolayer of Fe. We have shown that the data of reference [12], although implying large momentum transfers, can be qualitatively interpreted in terms of the widely used dipole approximation, due to the flatness of the filled Ni d bands. We have analysed the structures appearing in the loss spectrum of the clean surface in terms of electronic transitions involving surface states and/or surface-modified bulk states. The latter transitions yield a relevant contribution to the surface dielectric function, which determines the loss processes in the conditions of reference [12]. The observed shoulder at $\simeq$ 10 eV is interpreted as the surface plasmon of Ni, while the weak structure at 20 eV is a remnant of the bulk plasmon. In spite of these names, it should be borne in mind that the whole loss function is here determined by the surface dielectric function. Strictly speaking, "bulk plasmon" here means that the surface dielectric function vanishes; hence, the plasmon of the surface sheet is excited. In a similar way, "surface plasmon" here means the plasmon of the (outer) vacuum-surface boundary. Finally, the changes of the loss probability upon adsorption of one monolayer of Fe, calculated by us, are in qualitative agreement with those observed experimentally.

We acknowledge the support of the following funding agencies: INFM (PRA 1MESS and Parallel Computing Initiative) and EU (NANOPHASE Research training network, contract No. HPRN-CT-2000-00167).

References

1. H. Ibach, D.L. Mills, *Electron energy loss spectroscopy and Surface Vibrations* (Academic Press, New York, 1982)
2. see, for a review, P. Chiaradia, R. Del Sole, Surf. Rev. Lett. **6**, 517 (1999)

3. A. Balzarotti, M. Fanfoni, F. Patella, F. Arciprete, E. Placidi, G. Onida, R. Del Sole, to appear in Surf. Sci. Lett.
4. A. Selloni, R. Del Sole, Surface Sci. **168**, 35 (1986)
5. P. Monachesi, R. Capelli, R. Del Sole, Eur. Phys. J. B **26**, 159 (2002)
6. G.M. Fehrenbach, Phys. Rev. B **59**, 15085 (1999)
7. E.E. Krasovskii, W. Schattke, Phys. Rev. B **63**, 235112 (2001)
8. see reference [7] and references therein
9. J. Wills, B.R. Cooper, Phys. Rev. B **36**, 3809 (1987)
10. O.K. Andersen, Phys. Rev. B **12**, 3060 (1975)
11. P. Monachesi, M. Palummo, R. Del Sole, R. Ahuja, O. Eriksson, Phys, Rev. B **64**, 115421 (2001)
12. S. D'Addato, L. Pasquali, G.C. Gazzadi, R. Verucchi, R. Capelli, S. Nannarone, Surf. Sci. **454-456**, 692 (2000)
13. J.D.E. McIntyre, D.E. Aspnes, Surf. Sci. **24**, 417 (1971)
14. P. Hohenberg, W. Kohn, Phys. Rev. B **136**, 864 (1964); W. Kohn, L.J. Sham, Phys. Rev. **140**, A1153 (1965)
15. U. von Barth, L. Hedin, J. Phys. C **5**, 1629 (1972)
16. A. Marini, G. Onida, R. Del Sole, Phys. Rev. B **64**, 195125 (2001)
17. D.G. Dempsey, W.R. Grise, L. Kleinman, Phys. Rev. B **18**, 1550 (1978)
18. T.J. Kreutz, T. Greber, P. Aebi, J. Ostenwalder, Phys. Rev. B **58**, 1300 (1998)
19. R. Car, M. Parrinello, Phys. Rev. Lett. **55**, 2471 (1985)
20. F. Bassani, G. Pastori Parravicini, *Electronic states and optical transitions in solids* (Pergamon, Oxford, 1975)
21. O. Jepsen, O.K. Andersen, Solid State Comm. **9**, 1763 (1971)
22. P.B. Johnson, R.W. Christy, Phys. Rev. B **9**, 5056 (1974)
23. A. Delin, Ph.D. thesis, Uppsala University 1998, p. XII-5
24. F. Manghi, R. Del Sole, A. Selloni, E. Molinari, Phys. Rev. B **41**, 9935 (1990)
25. R. Del Sole, in *Photonic Probes of Surfaces*, edited by P. Halevi (Elsevier, 1995), p. 152
26. E. Colavita, M. De Crescenzi, L. Papagno, R. Scarmozzino, L.S. Caputi, R. Rosei, E. Tosatti, Phys. Rev. B **25**, 2490 (1982)
27. R. Wu, A.J. Freeman, Phys. Rev. B **45**, 7205 (1992)
28. A. Theobald, V. Fernandez, O. Schaff, Ph. Hoffmann, K.-M. Schindler, V. Fritzsche, A.M. Bradshaw, D.P. Woodruff, Phys. Rev. B **58**, 6768 (1998)
29. G.C. Gazzadi, F. Bruno, R. Capelli, L. Pasquali, S. Nannarone, Phys. Rev. B **65**, 205417 (2002)